



**Fermi National Accelerator Laboratory**

FERMILAB-Conf-79/085-E

**A SEARCH FOR DIRECT PHOTON PRODUCTION AT FERMILAB ENERGIES  
AND COMPARISON WITH DIRECT PHOTON MEASUREMENTS  
AT ISR ENERGIES**

**B. Cox**

**December 1979**

**(Presented at the International Symposium on Lepton and Photon  
Interactions at High Energies, Fermilab, August 23-29, 1979)**



A SEARCH FOR DIRECT PHOTON PRODUCTION AT FERMILAB ENERGIES  
AND COMPARISON WITH DIRECT PHOTON MEASUREMENTS AT ISR ENERGIES

B. Cox

Fermi National Accelerator Laboratory  
Batavia, Illinois 60510 U.S.A.

Abstract

A search for direct photon production has been performed at Fermilab in 200 and 300 GeV/c Proton-Be interactions over a wide range of  $X_F$  and  $P_{\perp}$ . An excess of photons has been detected which when interpreted as single photon production yields a  $\gamma/\pi^0$  ratio which averages  $.070 \pm .025$  in the region  $1.5 < P_{\perp} < 4.0$  GeV/c and  $-.7 < X_F < .0$ . This measurement is discussed and a comparison of this result with the ISR measurements of the  $\gamma/\pi^0$  ratio has been made in an attempt to infer the energy dependence of direct photon production.

1. Introduction

Prior to the 1977 Lepton-Photon Conference in Hamburg, considerable interest had been aroused by the possibility<sup>1-2</sup> that photons could be produced directly in hadron-hadron collisions by the interactions of the constituents of the nucleons. At the 1977 conference, the two pieces of data which existed at the time were presented<sup>3</sup>. This data is shown in Fig. 1. Since that

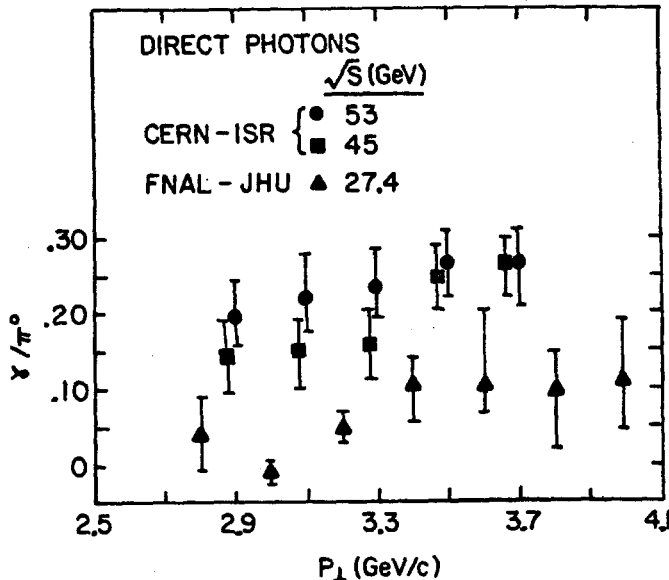


Fig. 1 Measured  $\gamma/\pi^0$  ratio as a function of  $P_{\perp}$  at the time of the 1977 Lepton-Photon Conference.

time, efforts to detect a direct photon signal have intensified. The ISR measurements<sup>4</sup> have been superseded by new ISR experiments<sup>5-7</sup> and the early result of Ref. 4 is now considered to be an upper limit determination. The Fermilab-JHU experimenters have performed a new and improved search<sup>8</sup> with 200 and 300 GeV/c proton beams. We will discuss this new experiment and compare the results with the new ISR experiments. Finally, several new theoretical calculations<sup>9-13</sup> of the level of direct photon production arising from QCD Compton scattering of gluons, QCD quark-antiquark annihilation, and the CIM virtual meson process (shown in Fig. 2a, b, and c respectively) have been performed. Some comparisons of the observed  $\gamma/\pi^0$  ratios with the predictions of these

\*Operated by Universities Research Association, Inc., under contract with the U. S. Department of Energy.

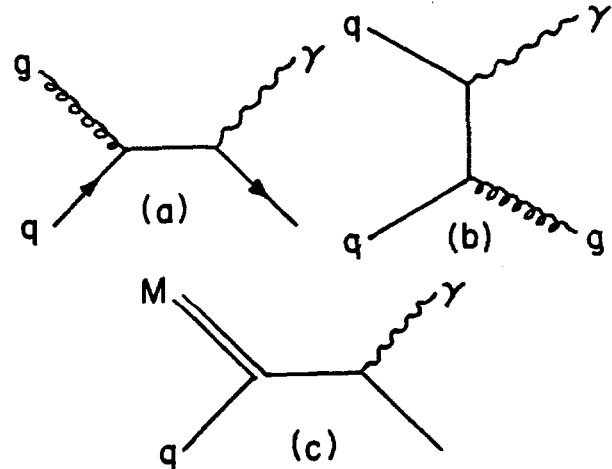


Fig. 2 a) Direct photon production by gluon-quark Compton scattering. b) Direct photon production by quark-antiquark annihilation. c) Direct photon production by CIM meson-quark scattering.

models will be made.

2. Direct Photon Production in 200 and 300 GeV/c pBe Interactions

The measurement<sup>8</sup> which is described in this section was performed in the P-West branch of the Proton area of Fermilab by a Fermilab-JHU collaboration using the lead glass spectrometer shown in Fig. 3. This experiment, which was conducted over a wide range of  $P_{\perp}$  and  $X_F$  (300 GeV region of measurement shown in Fig. 3) by varying the spectrometer arm angles over a large range of  $\theta_{cms}$ , consisted of the four distinct measurements listed below:

- 1) Measurement of the total "single photon" flux. By "single" we mean all signals including coalescing  $\pi^0$ , and neutral hadrons which simulate a single photon shower.
- 2) Measurement of  $\pi^0$  production in the same kinematic region by detecting both of the decay photons and reconstructing their energy and position.
- 3) Measurement of the  $\eta^0/\pi^0$  ratio (This could only be performed near  $X_F = 0$  because of the limited acceptance for  $\eta$ 's at larger center of mass angles).
- 4) Measurement of the ratio of neutral hadron to "single photon" flux.

In the case of all of these measurements, each spectrometer arm was triggered independently. The trigger consisted of the requirement of a neutral particle which was imposed by demanding no signal in the lucite hodoscopes L1, L2, and L3 in front of the Pb glass arrays and the requirement of total energy in the Pb glass above trigger threshold. The measurements of

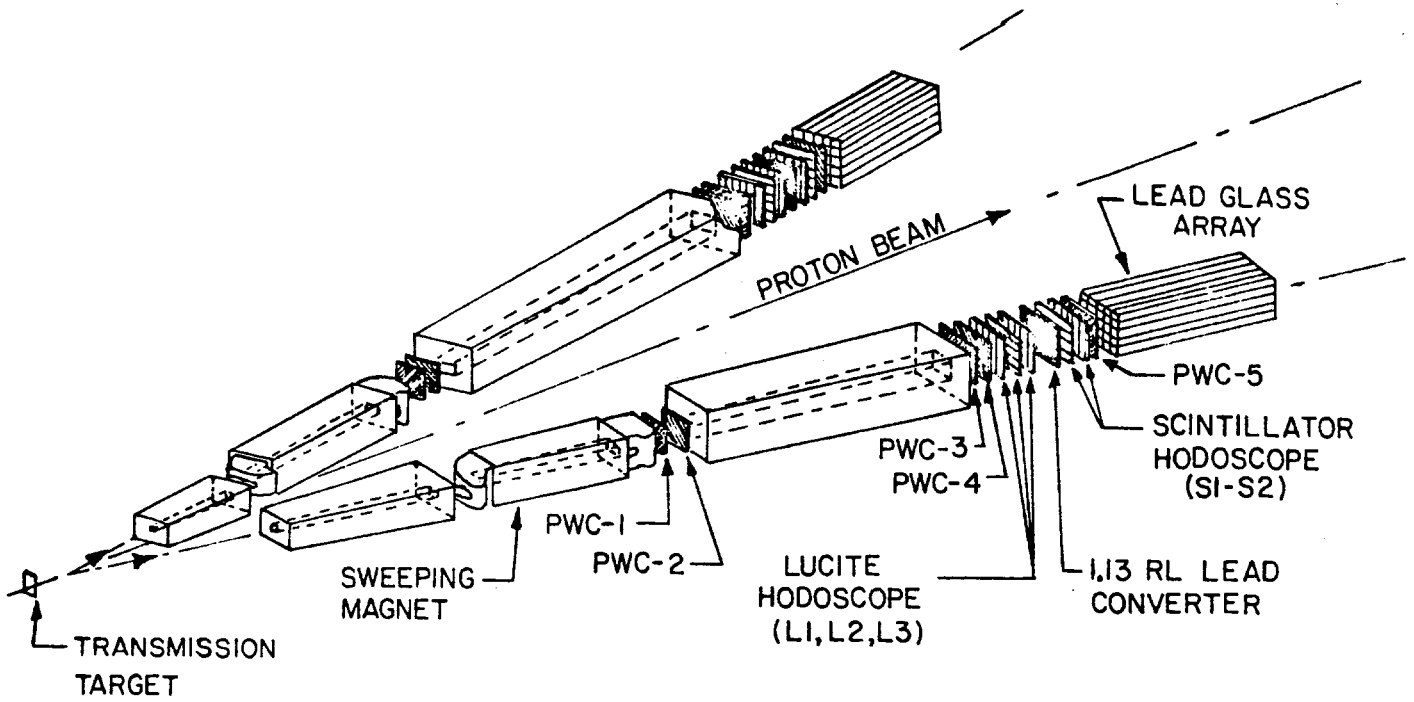


Fig. 3 Schematic view of the double arm photon spectrometer.

"single photons",  $\pi^0$ 's, and the  $\eta^0/\pi^0$  ratio were performed simultaneously. A typical  $\pi^0$  spectrum is shown in Fig. 4 and the  $\eta^0$  production data which was accumulated is shown in Fig. 5. As noted in Fig. 5 the  $\eta^0/\pi^0$  ratio obtained from this data is  $.47 \pm .10$  in good agreement with other measurements<sup>14</sup> at 200 GeV/c and slightly smaller than the ISR measurements<sup>15-17</sup> performed at higher energies.

The measurement of the neutral hadron component of the neutral flux required a separate run at each spectrometer angle and energy. In order to eliminate the photons, 11.3 radiation length of lead were inserted in the apertures of both arms during these runs. The flux of non-interacting neutral hadrons which penetrated the lead and triggered the spectrometer were then corrected for a 31% attenuation due to interactions in the lead. This attenuation was calculated from the measured total cross sections<sup>18</sup> for hadrons in lead. Typical ratios of neutral hadron to total neutral flux as a function of  $P_{\perp}$  are shown in Fig. 6 for two laboratory angle settings

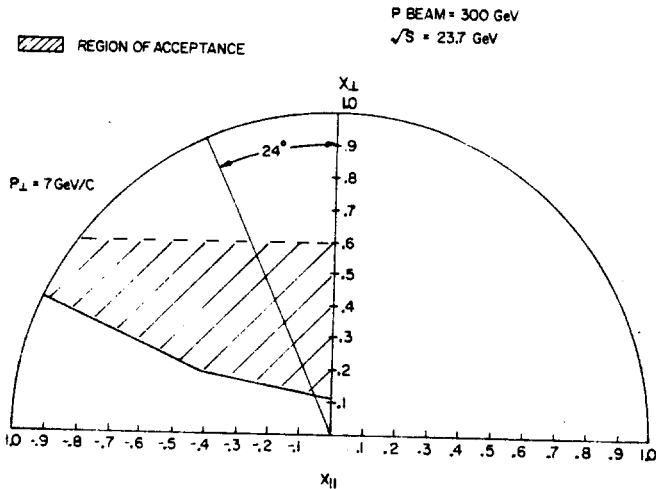


Fig. 4 Shaded region is the region of acceptance at 300 GeV. The acceptance of the spectrometer at a single forward angle setting of the spectrometer ( $\sim 6^\circ$  in the laboratory) is indicated by the  $24^\circ$  cms slice.

of the spectrometer arms. This ratio was determined as a function of  $X_F$  and  $P_{\perp}$  and subtracted in each  $X_F$  and  $P_{\perp}$  bin from the observed "single photon" flux.

The results of the measurement of the  $\pi^0$  flux over the range  $.1 < X_{\perp} < .5$  and  $-.8 < X_F < .0$  are shown in Figs. 8, 9, and 10 and are described in Ref. 19. At both 200 and 300 GeV/c the data fit the form

$$E \frac{d\sigma}{dp^3} = A P_{\perp}^{-N} (1-X_R)^M \quad (1)$$

with  $N = 8.9 \pm 1.1$  and  $M = 4.9 \pm 2.2$ . As shown by the product spectra  $P_{\perp}^N \cdot E \frac{d\sigma}{dp^3}$  and  $(1-X_R)^M \cdot E \frac{d\sigma}{dp^3}$  in Figs. 8 and 9, the cross sections exhibit scaling with energy and show no flattening of the  $P_{\perp}$  spectrum in the  $X_{\perp}$  range in which ISR experiments<sup>20,21</sup> have observed a change in the  $P_{\perp}$  exponent. The flatness of the product  $P_{\perp}^N \cdot E \frac{d\sigma}{dp^3}$  vs.  $\theta_{\text{cms}}$  shown in Fig. 10 gives further confirmation of the correctness of equation (1). This data supplies the basis for the denominator of the  $\gamma/\pi^0$  ratio.

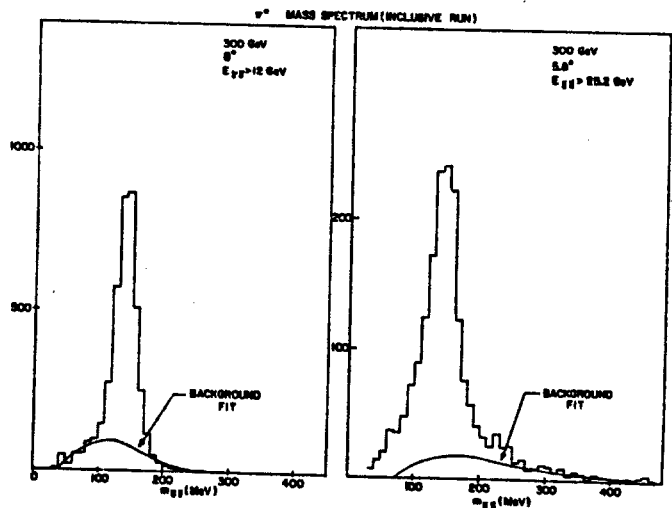


Fig. 5 Two "typical"  $\pi^0$  mass spectra and estimates of backgrounds.

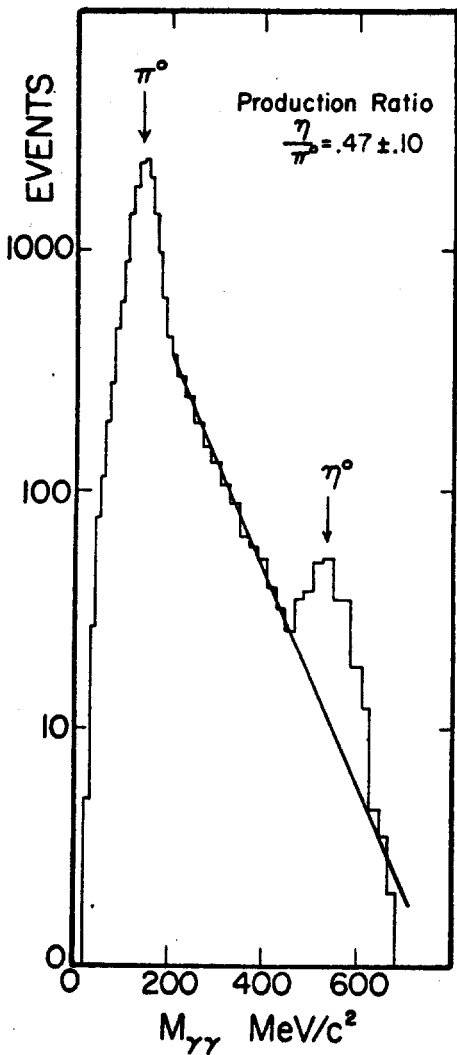


Fig. 6  $\eta$  production mass spectrum.

$R_H = \frac{\text{BACKGROUND FROM NEUTRAL HADRONS}}{\gamma \text{ CANDIDATES}}$

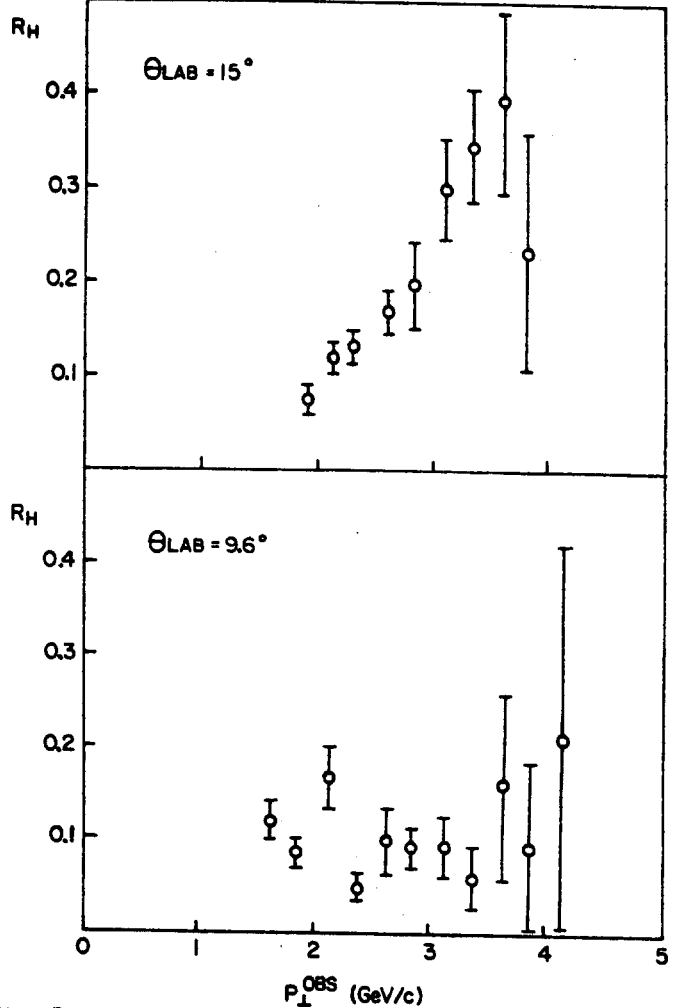


Fig. 7 Measured ratio of neutral hadron production to total "single photon" candidates.

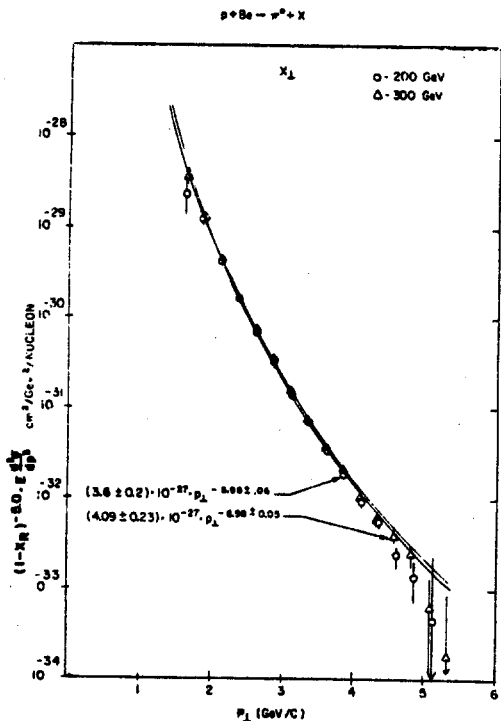


Fig. 8  $(1-X_R)^{-5} \cdot E \frac{d\sigma}{dp_3}$  vs.  $P_1$  displays the explicit  $P_1$  dependence of the data.

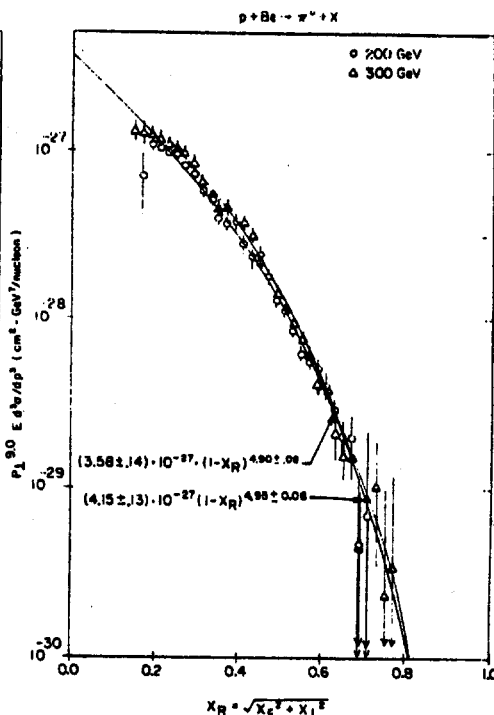


Fig. 9  $P_1^9 \cdot E \frac{d\sigma}{dp_3}$  vs.  $X_R$  displays the explicit  $(1-X_R)$  dependence of the data.

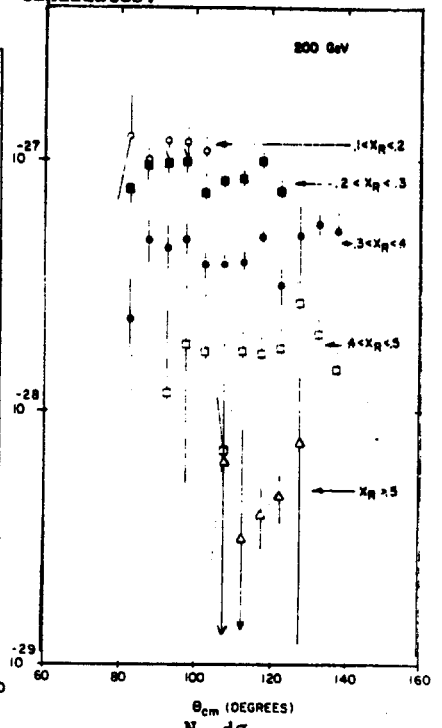


Fig. 10  $P_1^N \cdot E \frac{d\sigma}{dp_3}$  vs.  $\theta_{\text{cms}}$  demonstrates the  $\theta_{\text{cms}}$  independence of the data.

The explicit method for calculating the  $\gamma/\pi^0$  ratio in any  $X_F$  and  $P_\perp$  bin is given by

$$\frac{\gamma}{\pi^0} = \frac{\epsilon(\pi^0)}{\epsilon(\gamma)} \cdot \frac{N_Y - N_Y^{MC}}{N_{\pi^0}} \quad (2)$$

- where  $N_Y$  = Number of observed photons (neutral hadrons subtracted).
- $N_{\pi^0}$  = Number of observed  $\pi^0$  (background two photon combinations subtracted).
- $N_Y^{MC}$  = Number of predicted single photon-like events.
- =  $N_{\eta \rightarrow \gamma} + N_{\pi^0 \rightarrow \gamma} + N_{\text{coalescing } \pi^0}$
- $\epsilon(\pi^0)$  = Acceptance of the spectrometer arms as a function of  $X_F$  and  $P_\perp$  for  $\pi^0$  events.
- $\epsilon(\gamma)$  = Acceptance of the spectrometer arms as a function of  $X_F$  and  $P_\perp$  for direct  $\gamma$ .
- with  $N_Y^{MC} = W_Y^{MC} \cdot \frac{N_{\pi^0}}{W_{\pi^0}^{MC}}$  (3)
- $W_Y^{MC}$  = Monte Carlo weight of accepted single photon-like events predicted from the three sources.
- $\frac{N_{\pi^0}}{W_{\pi^0}^{MC}}$  = Ratio of the number of observed pizero's in a given normalization region to the Monte Carlo calculated weight of the accepted  $\pi^0$  events predicted in the normalization region.

The essence of the technique for detecting a direct photon signal in this experiment is the observation of  $\eta$  and  $\pi^0$  signals and the prediction of the level of single photons which should be in a given  $X_F$  and  $P_\perp$  bin via a Monte Carlo duplicating all observed features of the  $\pi^0$  and  $\eta$  flux. The single photon flux, as previously indicated, consists of four components, namely single photons from  $\pi^0$  and  $\eta^0$  decay, single photons from coalesced  $\pi^0$  events, and neutral hadrons which simulate a high energy photon. The Monte Carlo normalized to the observed  $\pi^0$  flux and containing  $\eta$ 's in the proper ratio to the  $\pi^0$ 's was used to predict the first three of these components. The detector was simulated in great detail and the lead glass energy distributions predicted by the Monte Carlo were passed through the same pattern recognition and analysis program to ensure similar treatment of real and simulated events. The Monte Carlo shower patterns in the array were adjusted to agree with the distribution of electron showers measured during the calibration of the detectors in the P-West calibration electron beam.<sup>22</sup> Fig. 11a and 11b show the size of the four components of the "single photon" spectrum for a typical piece of data versus  $X_F$  and  $P_\perp$ . An excess of some hundreds of events is observed for this particular data sample.

In order to assign errors to the final  $\gamma/\pi^0$  ratio calculated in the manner described above, many possible sources of systematic error were investigated. These sources are listed in Table I along with their contributions to the uncertainty in the ratio.

Table I

Error in the determination of the number of $\pi^0$ 's in the data samples (Background subtraction)	$\pm .016$
Error due to energy non-linearities in the detector	$\pm .007$
Error due to systematic shifts in energy of converting photons	$+ .007$ $- .016$
Error due to possible variation of $\pi^0$ Monte Carlo	$+ .018$ $- .004$
Error due to pattern recognition differences between data and Monte Carlo	$+ .010$ $- .010$
Error due to error in the conversion probability	$\pm .005$
Error due to error in the $\eta/\pi^0$ ratio	$+ .007$ $- .002$
Others	$< .005$

Total Systematic Error  $\sim .025$

The total systematic error dominates the error in the average value of  $\gamma/\pi^0 = .070 \pm .025$  found for the entire region of acceptance averaging over both the 200 and 300 GeV/c data. The systematic error is approximately the same as the statistical errors on individual bins in the plots of  $\gamma/\pi^0$  vs.  $P_\perp$ ,  $X_F$ ,  $X_R$  and  $\theta$  which are displayed in Figs. 11a, 11b, 12a and 12b respectively. The systematic uncertainty is shown as a band within which the data can be raised or lowered. The error bars on the data include both the statistical error and the error in the determination of the neutral hadron background. The spectrometer arms in this experiment are different lengths and because of this the systematic effects as well as the contributions of the various components of the "single photon" spectrum to the total spectrum differ for the arms. The data from each arm has been analyzed separately and the  $\gamma/\pi^0$  ratio agrees within the assigned errors. A more detailed discussion of these systematic effects is given in Ref. 8.

The excess of single photons which was observed in this experiment when interpreted as direct photon production give the  $\gamma/\pi^0$  ratio shown in Figs. 12a, 12b, 13a, and 13b.

These results indicate that  $\gamma/\pi^0$  is increasing as a function of  $P_\perp$  and  $X_F$ . However, it should be emphasized that the values of  $\gamma/\pi^0$  given in these plots are average over the region of observation (see Fig. 3) and therefore cannot directly be compared with the theoretical predictions which are typically for  $90^\circ$  in cms. In particular, since some increase of  $\gamma/\pi^0$  with  $X_F$  is observed experimentally, the level of  $\gamma/\pi^0$  vs.  $P_\perp$  might be expected to be raised and flattened by the averaging over a finite angle region. The statistical level of the data sample did not allow the detailed study of  $\gamma/\pi^0$  vs.  $P_\perp$  in bands of  $X_F$  which would be needed in order to cleanly separate the  $X_F$  and  $P_\perp$  behavior. Ignoring these two problems in making the comparison of data and theory, we show in Fig. 12a four

theoretical predictions for the level of  $\gamma/\pi^0$  at these low energies. Curve a is the prediction of Rückel, Brodsky, and Gunion<sup>10</sup> for  $\gamma/\pi^0$  ratio at 200 and 300 GeV/c. This prediction includes both QCD and CIM effects, uses a calculated  $\pi^0$  cross section for the denominator, and is valid, strictly speaking, only for  $90^\circ$ . Curve b is the QCD calculation of Halzen and Scott<sup>23</sup> which includes both diagrams 2a and 2b but fixes the absolute level of the direct photon production not by using the normal value of  $\alpha_s$ , the running QCD coupling constant, but rather by normalizing to the level of high mass dimuon production<sup>24</sup> (which proceeds via virtual photons by the same diagrams). If the usual  $\alpha_s$  is used, curve b would be lowered by a factor of 2.5. Curve c is the sum of a CIM calculation performed by Halzen and Scott and curve b. The denomi-

ator of the  $\gamma/\pi^0$  ratio of both curve b and curve c is experimental data and the prediction is a  $90^\circ$  calculation. Finally curve d is the QCD calculation of Contogouris et al.<sup>12</sup>. Once again, the calculation is for  $90^\circ$  and the denominator is derived from experimental data. Notice that in this region the calculation is similar to that of Halzen and Scott except for normalization.

### 3. Comparison With Other Data

The theoretical predictions of the  $\gamma/\pi^0$  ratio suffer from many difficulties not only in the calculation of the direct photon production cross section but in an ambivalence of attitude about whether experimental data or a theoretical prediction should be used for the  $\pi^0$  production. In addition, most of the experiments inte-

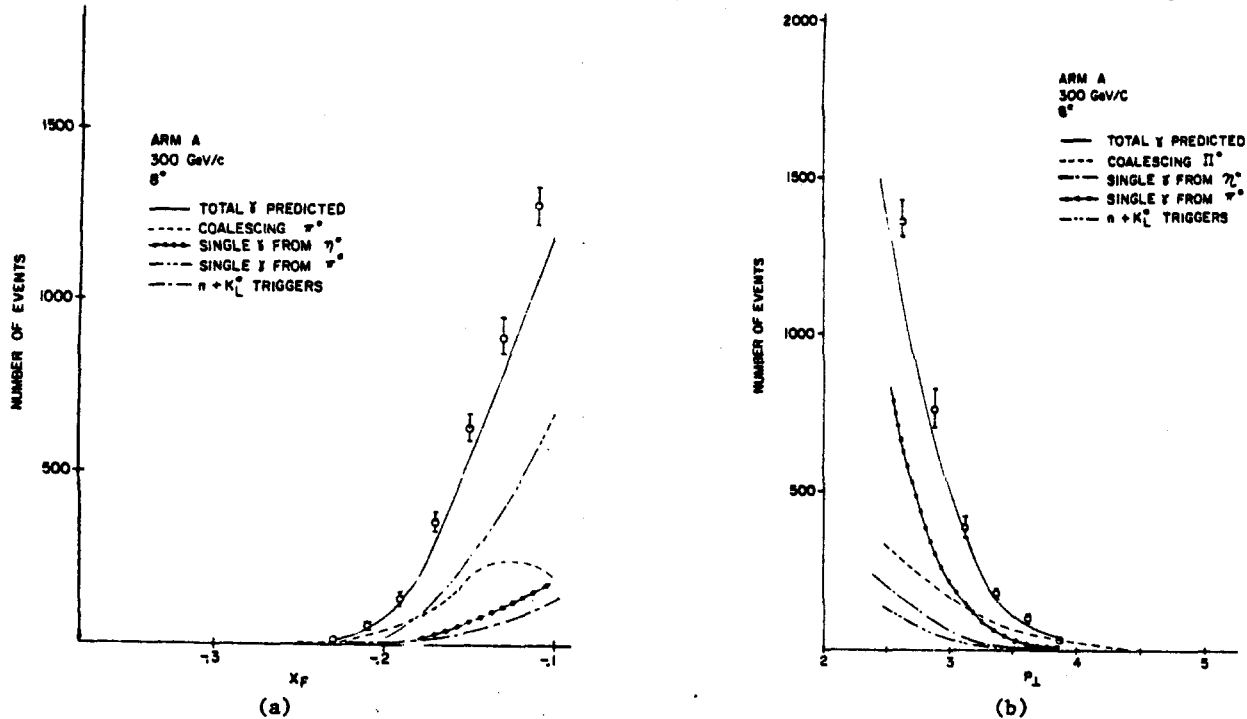


Fig. 11 The contributions of the four components of the raw "single photon" flux to the total number of events predicted at a spectrometer setting of  $8^\circ$  in the lab at 300 GeV/c. a) vs.  $X_F$  b) vs.  $P_\perp$ .

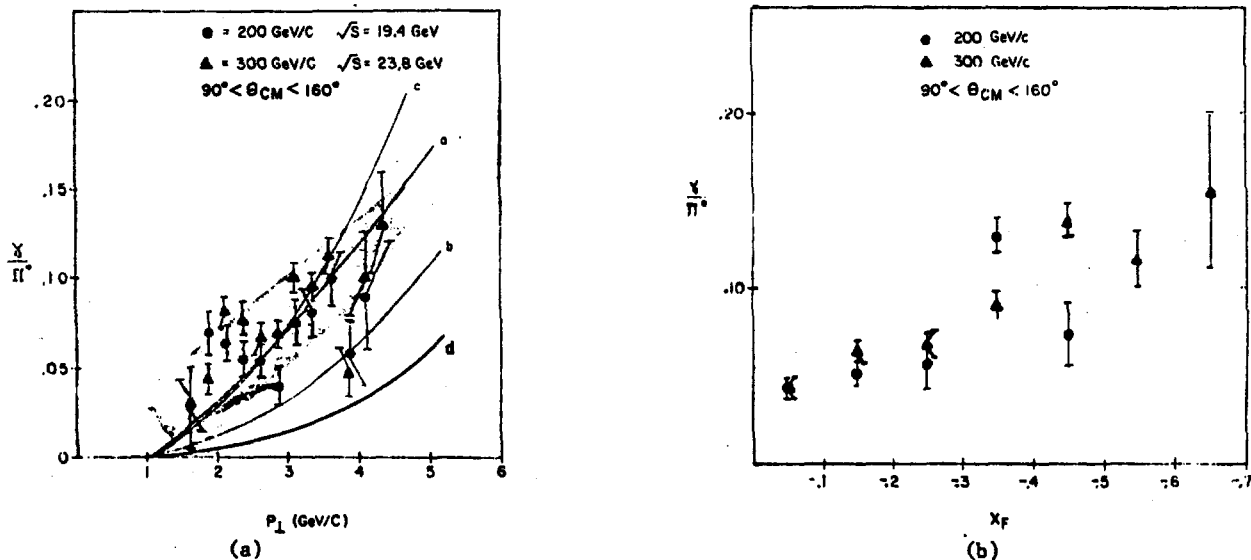


Fig. 12 The shaded bands indicate the magnitude of the systematic error. The level of the data may be shifted within the limit of the bands. a)  $\gamma/\pi^0$  ratio vs.  $P_\perp$  for 200 and 300 GeV pBe interactions; curve a is the prediction of Rückel, Brodsky and Gunion; curve b is the QCD calculation of Scott and Halzen; curve c is the summed QCD + CIM calculation of Halzen and Scott and curve d is the scale breaking QCD calculation of Contogouris et al. b)  $\gamma/\pi^0$  ratio vs.  $X_F$ .

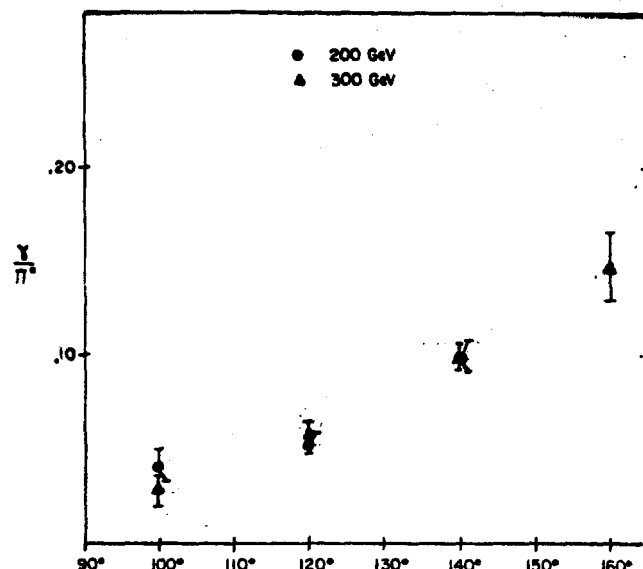
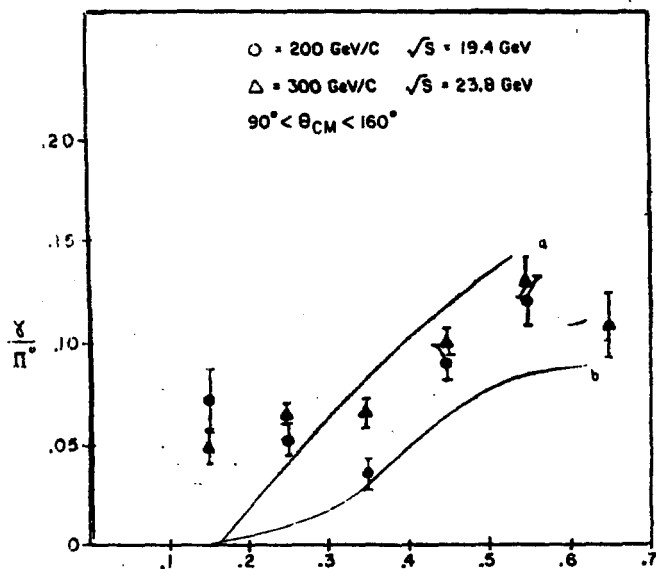


Fig. 13 a)  $\gamma/\pi^0$  ratio vs.  $X_R^{\text{Radial}}$  for 200 and 300 GeV pBe interactions. Curve a is the prediction of Rückel, Brodsky, and Gunion for the  $X_R$  dependence of  $\gamma/\pi^0$ ; curve b is the QCD prediction of Halzen and Scott. b)  $\gamma/\pi^0$  ratio vs.  $\theta_{\text{CMS}}$ .

grate or average over a non-zero angular range by nature of the acceptance of the various detectors. These facts coupled with the different energy ranges of the existing experiments make the comparison of the various data sets difficult since not even a theoretical guide exists which would allow the data to be put on common footing.

However, some attempts can be made to look for trends in the data. Following suggestions by Halzen and Scott<sup>23</sup> and previous experience with  $\pi^0$  production, if direct photon production can be factored into a function of  $P_{\perp}$  and  $X_{\perp}$  like  $\pi^0$  production, we can write

$$\frac{\gamma}{\pi^0} = \frac{(E \frac{d\sigma}{dp})_{\gamma}}{(E \frac{d\sigma}{dp})_{\pi^0}} \sim \frac{P_{\perp}^{N'} g(X_{\perp})}{P_{\perp}^N f(X_{\perp})} \sim P_{\perp}^{N'-N} Q(X_{\perp})$$

and  $\frac{\gamma}{\pi^0}$  itself is a factorizable function of  $X_{\perp}$  and  $P_{\perp}$ . In order to organize the thinking about this formula, we will investigate three possible forms that this formula can take.

1.  $N=N'$   $\rightarrow \frac{\gamma}{\pi^0} \sim P_{\perp}^{N'-N}$  pure  $P_{\perp}$  dependence - ratio independent of  $X_{\perp}$   
 $g(X_{\perp})=f(X_{\perp})$
2.  $N=N'$   $\rightarrow \frac{\gamma}{\pi^0} \sim Q(X_{\perp})$  pure  $X_{\perp}$  dependence - ratio independent of  $P_{\perp}$   
 $g(X_{\perp})=f(X_{\perp})$
3.  $N=N$   $\rightarrow \frac{\gamma}{\pi^0} \sim P_{\perp}^{N'-N} Q(X_{\perp})$   
 $g(X_{\perp})=f(X_{\perp})$

The first two cases are extreme cases and case 3 encompasses all the possibilities in between. By ignoring the differences of angular range encompassed by the various experiments and ignoring possible A dependence effects in comparing the fixed target experiment and the ISR data we can check these possibilities.

In order to check possibility 1, we plot  $\gamma/\pi^0$  at a fixed  $P_{\perp}$  as a function of  $\sqrt{s}$  of the interaction.

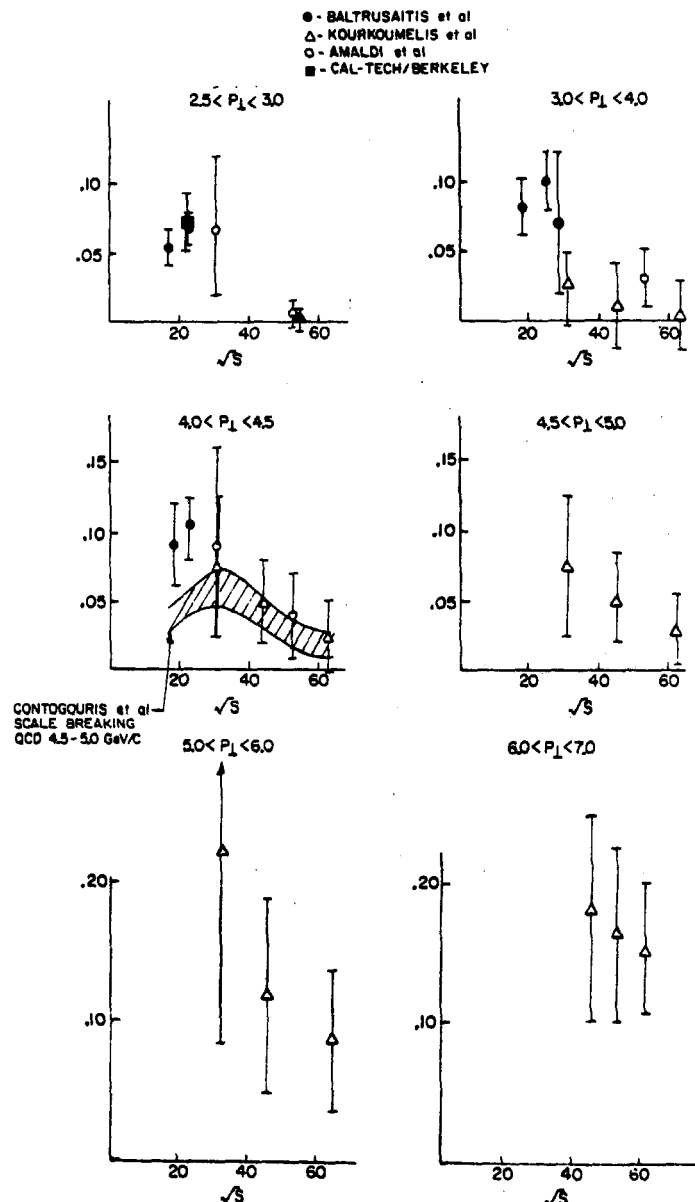


Fig. 14  $\gamma/\pi^0$  vs.  $\sqrt{s}$  at fixed  $P_{\perp}$ .

BALTRUSAITIS et al	19.4	○
	23.8	●
AMALDI et al	31	△
	53	▲
KOURKOUHELIS et al	31	□
	45	■
	62	X

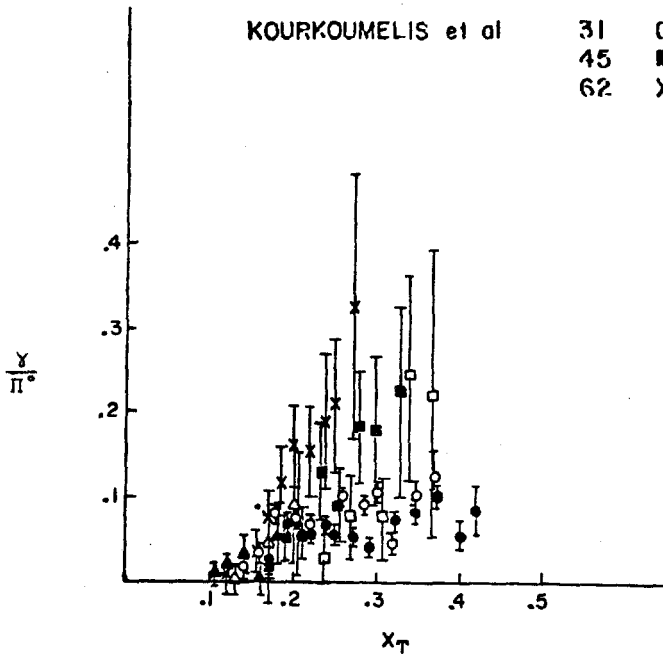


Fig. 15  $\gamma/\pi^0$  vs.  $X_L$ .

If the ratio is a function only of  $P_\perp$  then the  $\gamma/\pi^0$  ratio should be independent of energy. The data is shown in Fig. 14. With the underlined caveats the ratio seems to decrease with  $\sqrt{s}$  at fixed  $P_\perp$ .

We have compared the energy dependence of the QCD calculation of Contogouris et al. to the data in the  $4 < P_\perp < 4.5$ . The prediction is below the data at low  $\sqrt{s}$  (remember that the angular range of the data for the low energy points in  $90^\circ < \theta < 160^\circ$  as compared to  $90^\circ < \theta < 100^\circ$  for Kourkoumelis et al.) but in general a fall off of  $\gamma/\pi^0$  with  $\sqrt{s}$  at fixed  $P_\perp$  seems to be predicted. The theory of Rückel et al. would predict no  $\sqrt{s}$  dependence.

In order to check possibility 2 we have plotted the various data as a function of  $X_L$ . This is shown in Fig. 15. From this data one can see that there is no universal function of  $X_L$ . At a fixed  $X_L$  the data indicates quite clearly that the  $\gamma/\pi^0$  ratio increases.

Finally, since neither of the two simple possibilities seem to be indicated, an attempt can be made to investigate more complicated cases. The data indicates that the  $\gamma/\pi^0$  ratio is rising slowly at a given energy with  $P_\perp$ . Therefore  $N'-N > 0$  but not large. If we assume  $N'-N-1$ , by plotting  $\frac{\gamma}{\pi^0} \cdot P_\perp^{-1}$  vs.  $X_L$  we can check to determine if the data lie on some universal function of  $X_L$ . This is shown in Fig. 16. Once again we are disappointed. While the higher  $X_L$  data tends to line up, the lower  $X_L$  data seems to disperse a bit. No simple answer is evident at this time with the existing data.

BALTRUSAITIS et al	19.4	●
	23.8	○
AMALDI et al	31	△
	53	▲
KOURKOUHELIS et al	45	□
	53	■
	62	X

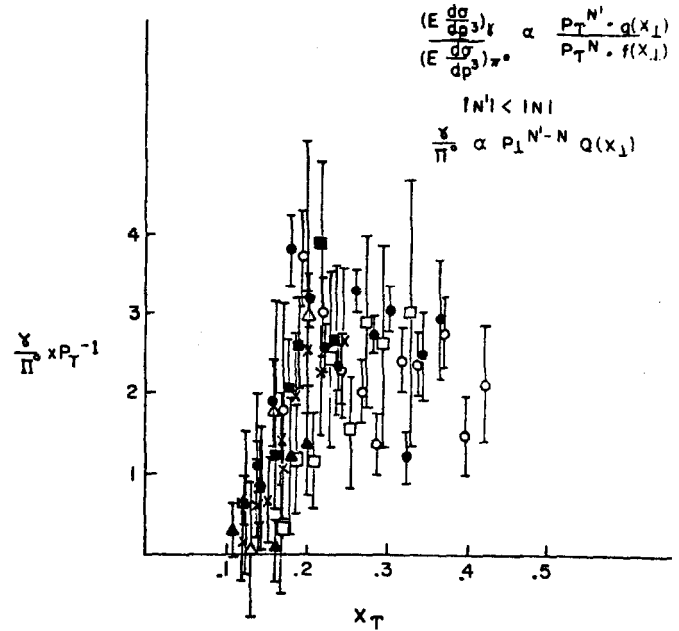


Fig. 16  $\frac{\gamma}{\pi^0} \cdot P_\perp^{-1}$  vs.  $X_L$ .

#### 4. Conclusions

What inferences can we draw from these data? First and foremost, there is an excess of single photons above that which we can expect from  $\eta$  and  $\pi^0$  decay. In addition, direct photon production is expected to be present and (at least in some calculations) copious enough to supply this excess. The  $\gamma/\pi^0$  ratio which is calculated from this excess is

$$\frac{\gamma}{\pi^0} \sim \begin{matrix} .065 \pm .025 & \sqrt{s} = 19.4 \\ .076 \pm .025 & \sqrt{s} = 23.8 \end{matrix}$$

$$1.5 < P_\perp < 4.0 \text{ GeV}/c$$

$$90^\circ < \theta_{\text{cms}} < 160^\circ$$

This  $\gamma/\pi^0$  signal seems to increase slowly with  $P_\perp$  and  $X_L$  although a clean separation of  $X_F$  and  $P_\perp$  dependence is not possible with existing data. If we compare the Fermilab data with the CERN ISR results,  $\gamma/\pi^0$  seems to decrease at fixed  $P_\perp$  (for the moderate  $P_\perp$  range  $< 5.0 \text{ GeV}/c$ ). However, a flat  $P_\perp$  dependence is not ruled out because comparison of different experiments complicated by different kinematic ranges of measurements, possible A effects, and differences in data sample which could arise because of different charge particle vetos for different experiments. In general,  $\gamma/\pi^0$  seems to increase with energy at a fixed  $X_L$  beyond  $X_L \sim .2$ . No signal has been observed by any experiment below  $X_L = .1$ .

Finally, in closing, it should be obvious that progress has been made since the Hamburg Conference. It should be equally obvious that more and better experiments are needed. It is to be hoped that by the next Lepton-Photon Conference outstanding questions about this exciting new process may be resolved.

#### Acknowledgements

The members of the Fermilab-JHU group which performed the 200/300 GeV/c measurement described in the talk are R. M. Baltrusaitis, M. Binkley, B. Cox, T. Kondo, C. T. Murphy, W. Yang, L. Ettlinger, M. S. Goodman, J.A.J. Matthews, and J. Nagy. I would also like to thank L. Madansky, D. Scott, F. Halzen, S. J. Brodsky, and A. P. Contogouris for many helpful comments. This work was supported by the United States Department of Energy, the Research Corporation, and the National Science Foundation.

#### References

1. G. R. Farrar and S.C. Frautschi, Phys. Rev. Lett. 36, 1017 (1976).
2. G. R. Farrar, Phys. Lett. 67B, 337 (1977).
3. J. Cronin, Hadron Induced Leptons and Photons, Proceedings-1977 Lepton-Photon Conference, 579 (1977).
4. P. Darriulat et al., Nucl. Phys. B110, 365 (1976).
5. J. H. Cobb et al., Phys. Lett. 78B, 519 (1978).
6. E. Amaldi et al., Phys. Lett. 84B, 360 (1979).
7. H. Diakonou et al., to be published Physics Letters, P. Mouzourakis, this conference.
8. R. M. Baltrusaitis et al., to be published Physics Letters.
9. F. Halzen and D. M. Scott, Phys. Rev. Lett. 40, 1117 (1978).
10. R. Rückel, S. J. Brodsky, and J. F. Gunion, Phys. Rev. 18, 2469 (1978).
11. F. Halzen and D. M. Scott, Phys. Rev. 18, 3378 (1978).
12. A. P. Contogouris and S. Padopoulos, M. Hongoh, Phys. Rev. Lett. 19, 2607 (1979).
13. R. D. Field, CALT-68-688 preprint.
14. C. J. Donaldson et al., Phys. Rev. Lett. 40, 684 (1978).
15. K. Eggert et al., Phys. Lett. 74B, 267 (1978).
16. F. W. Büsser et al., Nucl. Phys. B106, 1 (1976).
17. C. Kourkouvelis et al., CERN EP/79-30, (April, 1978).
18. S. P. Denisov et al., Nucl. Phys. B61, 62 (1973).
19. R. M. Baltrusaitis et al., Inclusive  $\pi^0$  Production Over Large  $X_L$  and  $X_T$  Ranges in 200, 300, and 400 GeV/c Proton-Beryllium Interactions, Fermilab-Pub. 79/37-Exp., to be published Physical Rev. Letters.
20. A. L. S. Angelis et al., Phys. Lett. 79B, 505 (1978).
21. C. Kourkouvelis et al., CERN EP 79-29, 10 April, 1979.
22. B. Cox, et al., Fermilab Technical Memo No. TM-765 6038.00.
23. F. Halzen, D. Scott, Private Communication.
24. J. K. Yoh et al., Phys. Rev. Lett., 41, 684 (1978).